arXiv:astro-ph/9905137v1 12 May 1999

The K–band Luminosity Function in Galaxy Clusters to $z \sim 1$

Roberto De Propris
School of Physics, Department of Astronomy & Optics, University of New South Wales, Sydney, Australia, NSW 2052; propris@edwin.phys.unsw.edu.au

S. A. Stanford[1]
University of California at Davis, and the Institute of Geophysics and Planetary Physics, Lawrence Livermore National Laboratories, Livermore, CA, 94550; adam@igpp.llnl.gov

Peter R. Eisenhardt[1]
MS 169-327, Jet Propulsion Laboratory, California Institute of Technology, 4800 Oak Grove Drive, Pasadena, CA, 91109; prme@kromos.jpl.nasa.gov

Mark Dickinson[1]
Space Telescope Science Institute, Baltimore, MD, 21218; med@stsci.edu

Richard Elston[1]
Department of Astronomy, University of Florida, Gainesville, FL, 32611; elston@astro.ufl.edu

ABSTRACT

We present K–band luminosity functions for galaxies in a heterogeneous sample of 38 clusters at $0.1 < z < 1$. Using infrared–selected galaxy samples which generally reach 2 magnitudes fainter than the characteristic galaxy luminosity L^*, we fit Schechter functions to background–corrected cluster galaxy counts to determine K^* as a function of redshift. Because of the magnitude limit of our data, the faint-end slope α is fixed at -0.9 in the fitting process. We find that $K^*(z)$ departs from no–evolution predictions at $z > 0.4$, and is consistent with the behavior of a simple, passive luminosity evolution model in which galaxies form all their stars in a single burst at $z_f = 2(3)$ in an $H_0 = 65$ km s^{-1} Mpc^{-1}, $\Omega_M = 0.3$, $\Omega_\Lambda = 0.7(0)$ universe. This differs from the flat or negative infrared luminosity evolution which has been reported for high redshift *field* galaxy samples. We find that the observed evolution appears to be insensitive

[1]Visiting Astronomer, Kitt Peak National Observatory, National Optical Astronomy Observatories, which is operated by the Association of Universities for Research in Astronomy, Inc. (AURA) under cooperative agreement with the National Science Foundation.

to cluster X-ray luminosity or optical richness, implying little variation in the evolutionary history of galaxies over the range of environmental densities spanned by our cluster sample. These results support and extend previous analyses based on the color evolution of high redshift cluster E/S0 galaxies, indicating not only that their stellar populations formed at high redshift, but that the assembly of the galaxies themselves was largely complete by $z \approx 1$, and that subsequent evolution down to the present epoch was primarily passive.

Subject headings: galaxies: luminosity function, mass function — galaxies: formation and evolution — galaxies: clusters

1. Introduction

The predominance of early–type galaxies in clusters compared to the field is a clear sign that the evolution of galaxies depends on environment, but the physical mechanisms at work remain the subject of considerable debate. In particular, the question of when and how the most massive galaxies formed, and especially the origin of giant elliptical galaxies, is a topic of ongoing, vigorous theoretical and observational research. The traditional picture of elliptical galaxy formation (e.g., Eggen, Lynden-Bell & Sandage 1962) postulates a single burst of star formation at high redshift followed by passive evolution. The existence of a tight color–magnitude relation in nearby clusters (e.g., Bower, Lucey & Ellis 1992; De Propris et al. 1999) and the close correlation between galaxy mass and metallicity implied by the $\mathrm{Mg}_2 - \sigma$ relation (Bender, Burstein & Faber 1993) is explained naturally by a single, early episode of star formation. If more massive galaxies are more efficient at retaining supernova ejecta, they will have higher metallicities and therefore redder colors (Arimoto & Yoshii 1987). If the color–magnitude relation is driven primarily by metal abundance, then the scatter in galaxy colors around the mean locus provides constraints on the epoch of galaxy formation. Both Bower et al. (1992) and De Propris et al. (1999) conclude that the intrinsic scatter in the $U - V$ colors of Coma galaxies is consistent with high formation redshifts and/or extreme synchronization in the epoch of galaxy formation.

The picture outlined above may be overly simplistic. A population of blue galaxies is commonly encountered in clusters at moderate redshift, with almost no counterpart in present day systems (Butcher & Oemler 1984). High resolution imaging indicates that these blue galaxies are mostly late–type spirals undergoing starbursts (Dressler et al. 1994; Couch et al. 1998 and references therein), and suggests that the cluster S0 population is far less abundant at $z \sim 0.5$ than today (Dressler et al. 1997). It has been proposed that

the blue galaxies are the progenitors of cluster S0 galaxies (e.g. Couch & Sharples 1987). In agreement with this explanation of the Butcher-Oemler effect, some S0s in the present epoch appear to contain younger stellar populations (Bothun & Gregg 1990; Kuntschner & Davies 1998). However, the colors of the combined E and S0 populations in the core of clusters show little change, other than that expected from passive spectral evolution, out to $z \sim 1$, even among clusters of widely varying richness and X-ray luminosity (e.g., Stanford, Eisenhardt, & Dickinson 1998, hereinafter SED98).

Further complications in the monolithic collapse scenario arise if, as has recently been found in the Coma cluster by Jørgensen (1999), the mean ages and abundances of cluster early-types are anti-correlated. A relation between age and abundance could allow significant variations in the ages of the stellar populations in cluster early-type galaxies, while keeping the scatter in e.g. the color-magnitude relations small. A possible correlation between age and metallicity has been emphasized previously by Worthey, Trager, & Faber (1996), wherein the oldest galaxies are the most metal-poor. But recent work on the Fundamental Plane has found support for a scenario in which age varies *directly* with metallicity in elliptical galaxies, i.e. the most luminous ellipticals are the oldest and most metal rich, in a wide range of environments from the field to the Coma cluster (Pahre, De Carvalho, & Djorgovski 1998), suggesting that there still exists considerable controversy in such studies.

Hierarchical structure formation models present a very different view of galaxy evolution, in which galaxies assemble by a process of gradually merging smaller stellar systems over a wide range of redshifts (e.g., Cole et al. 1994). Some key factors governing the spectrophotometric evolution of elliptical galaxies in this scenario are the time at which the bulk of the stellar populations are formed, the era when the majority of mergers take place, and the amount of new star formation induced during each merging event in the construction of a large galaxy. If the formation of a large fraction of the stars in a giant elliptical galaxy is distributed over a broad cosmic time interval, then ellipticals at any redshift should exhibit a wide range in their mass–weighted stellar ages. If, however, most stars in present–day cluster ellipticals were formed in smaller disk galaxies at large lookback times ($z \gg 1$), and if little additional star formation takes place during subsequent mergers, then the end–product ellipticals could appear to be old and approximately coeval even if the bulk of the merging took place relatively late. The hierarchical models of Kauffmann & Charlot (1998a) reproduce the color–magnitude relation for ellipticals because more massive galaxies are the product of systematically more massive progenitors which retain more metals when forming their stars.

Discriminating between the formation scenarios described above is difficult, even by

studying galaxies in clusters at high redshift. The evolution of the color magnitude relation to $z \sim 1$ has been discussed by many workers in the field, e.g. Aragón-Salamanca et al. 1993, Lubin 1996, Ellis et al. 1997, and SED98. Most results are consistent with the high galaxy formation redshifts and subsequent passive evolution favored by monolithic collapse. But even the most comprehensive study spanning the largest redshift range, SED98, could not exclude the possibility that cluster ellipticals formed more recently from mergers of smaller galaxies, as long as the bulk of the stellar mass was created at much larger redshifts and there was little recent star formation in the subsequent merging process. Kauffmann & Charlot (1998a) have also argued that by selecting galaxies exclusively from rich clusters, studies such as those of Ellis et al. (1997) and SED98 introduce an increasingly strong bias at higher redshifts toward galaxies that have formed at earlier epochs, and therefore that the conclusions cannot be extended to the general cluster galaxy population today. An additional concern is that SED98 and Ellis et al. 1997 selected galaxies only from the densest core regions of clusters imaged by the *Hubble Space Telescope (HST).*

An alternative and potentially more powerful means of testing models of galaxy formation is to determine the mass function of galaxies over a large redshift range. The actual mass function is difficult to measure, although recent kinematic studies of the fundamental plane of cluster galaxies at high redshift (e.g. Kelson et al. 1997; van Dokkum et al. 1998) have made an important step in this direction. The K–band luminosity function (LF) may serve as a useful surrogate. Traditional optical LFs have been used as a sensitive probe of the bulk properties of galaxy populations both in the local universe (e.g., Binggeli, Sandage & Tammann 1988) and at high redshift (e.g. Lilly et al. 1995b; Ellis et al. 1996; Cowie et al. 1996). Although they are special environments, galaxy clusters are convenient to study because their luminosity functions can be measured without extensive spectroscopy by using statistical field galaxy subtraction. Infrared luminosities are particularly well suited for defining luminosity functions because they broadly reflect the total stellar mass of the galaxies, and do not depend strongly on the details of their stellar populations (Gavazzi, Pierini, & Boselli 1996). This allows us to study luminosity evolution at wavelengths where the mass–to–light ratio is comparatively insensitive to the star formation history (cf. Madau, Pozzetti, & Dickinson 1998). In addition, (i) the effects of extinction are much weaker at infrared wavelengths than in the optical; (ii) the infrared LF appears to be independent of environment (De Propris et al. 1998), and (iii) k–corrections for infrared colors are only weakly dependent on Hubble type and vary slowly with redshift (e.g., Poggianti 1997).

Luminosities derived from observed magnitudes depend on the assumed cosmology. In addition, cosmology affects the evolution of galaxy luminosities and colors by setting the relationship between lookback time and redshift. Jointly constraining the cosmological parameters, galaxy formation redshifts, and star formation histories is beyond the scope of

this paper. Therefore when comparing our data to evolutionary models we will constrain the discussion to a limited set of cosmologies. We adopt the parameters $\Omega_M = 0.3$ and $\Omega_\Lambda = 0.7$, with $H_0 = 65$ km s^{-1} Mpc^{-1} for consistency (Perlmutter et al. 1998; Riess et al. 1998), as our default cosmology. These high redshift supernovae results currently provide the strongest evidence for non-zero Λ cosmologies. In our analysis, we also consider more traditional $\Omega_M = 0.3$, $\Omega_\Lambda = 0.0$, and $\Omega_M = 1$, $\Omega_\Lambda = 0.0$ models.

In this paper we derive K–band LFs for a large sample of clusters at $0.1 \lesssim z \lesssim 1$. Since we remove field galaxy contamination statistically, we are sensitive to all morphological types and are not biased towards E/S0 galaxies over the covered magnitude range, unlike SED98 where the spiral and irregular galaxies were excluded. Our sample consists of the clusters reported in SED98, plus an additional set described below. We use the entire fields surveyed by our ground-based K–band imaging, rather than the smaller *HST* fields studied by SED98. The sample of 38 clusters spans a large range in several cluster properties and so may constitute a reasonably fair sample of cluster galaxy populations brighter than $K^* + 2$ over roughly half the age of the universe.

The structure of this paper is as follows. In section 2 we describe our observations and photometry. Section 3 discusses star–galaxy separation, statistical subtraction of field galaxies, and the derivation of the cluster luminosity functions. In section 4 we analyze the results and consider their implications for cluster galaxy evolution.

2. Observations, Data Reduction, and Photometry

The overall sample of clusters presented here is large and heterogeneous, consisting of 38 clusters at $0.14 < z < 0.92$, drawn from a variety of optical, X-ray, and radio selected samples. The redshift distribution of the whole sample is shown in Figure 1. As part of a survey more fully described in SED98, JHK_s images of the clusters were obtained using IR array cameras on NOAO telescopes at Kitt Peak and Cerro Tololo in 1993–1996. The lower redshift clusters were observed at the 2.1 m telescope at KPNO using IRIM, which has a 256×256 HgCdTe array with 1.09 arcsec pixels, and at the 1.5 m telescope at CTIO using CIRIM, which has a 256×256 HgCdTe array with 1.16 arcsec pixels, and OSIRIS, which had a 256×256 HgCdTe array with 0.95 arcsec pixels. The highest redshift clusters were observed at the 4 m telescope at KPNO using IRIM, where it has 0.6 arcsec pixels. Two of the clusters, Abell 370 and 851, were observed in 1991 with SQIID, which had 256×256 PtSi detectors with 1.30 arcsec pixels, as reported in Stanford, Eisenhardt & Dickinson 1995 (hereinafter SED95). The sample of clusters is summarized in Table 1, along with details on the observations such as the telescope/instrument, field size, and number of objects within

the field for each cluster.

Exposure times in all bandpasses were chosen to provide galaxy photometry with $S/N > 5$ for galaxies with the spectral energy distributions of present–day ellipticals down to ∼2 magnitudes fainter than L^* (unevolved) at the cluster redshift. This permits us to study galaxy properties over a similar range of luminosities for all clusters in our sample, regardless of their redshifts. Table 1 lists the K magnitude limit used to define the object sample for each cluster. Our images typically cover a field size of ∼1 to 1.8 Mpc at the cluster redshift; the actual field size is given in Table 1 for each cluster. The IR images were calibrated onto the CIT system wherein Vega has $m = 0$. The typical rms of the transformations is 0.03. The effective angular resolution of the images is generally limited by the large pixel scale of the infrared arrays, and is ∼1.7 arcsec for the $z < 0.6$ clusters and ∼1.2 arcsec for the more distant objects.

Object detection was carried out on the K images using a modified version (Adelberger, personal communication) of FOCAS (Valdes 1982), which was also used to obtain "total" magnitudes. The observing methods, data reduction techniques, and photometric methods for our ground–based data set are described in more detail in SED95. All photometry has been corrected for reddening using the interstellar extinction curve given in Mathis (1990), with values for $E(B-V)$ taken from Burstein & Heiles (1982).

3. Analysis

In order to derive LFs for our clusters, we need to remove contamination by stars in our Galaxy, and by background and foreground galaxies. Finally, we fit Schechter (1976) functions to the summed LF of the clusters in discrete redshift bins. We describe the procedures employed in the next three subsections.

3.1. Star-Galaxy Separation

The K–band images generally lack sufficiently high angular resolution to effectively distinguish stars from galaxies on the basis of image concentration or sharpness. Instead, we use color criteria and models. Huang et al. (1997) find that a line corresponding to the equation $(B-I) - 2.5\,(I-K) > -2$ separates stars and galaxies effectively in a color–color plane. Our cluster data do not always span such a large wavelength range; therefore we devise a different criterion based on infrared colors, which are available for all our objects.

As described in SED98, we used *HST* images to determine morphologies for objects

detected in our K–band images of a subset of the clusters in the whole sample. For this subsample, we plot $J-K$ vs. K in Figure 2. As is well known, stars generally lie in the region $J-K<1$ (e.g., Leggett 1992) whereas the k–correction for nearly all but the most local galaxies makes their observed $J-K>1$. To test this, we compare counts of stars in the $\sim$100 arcmin^2 IR field survey of Elston, Eisenhardt, & Stanford (1999; hereinafter EES) selected by the color criterion of Huang et al. (1997) with those selected using our $J-K$ criterion, and with Galaxy star count models from Bahcall & Soneira (1980, 1981), as modified for use in the infrared according to Mamon & Soneira (1982). Figure 3 plots star counts in the four fields of EES as a function of K. Star counts using our $J-K$ criterion and that of Huang et al. (1997) agree with each other and with the models, down to about $K=18$ (3 magnitudes brighter than the 5 σ level in the EES data), where both techniques overpredict the model star counts. At $K=18$, however, the field galaxy counts outnumber those of the stars in any of the EES fields by >10:1, and thus the details of the stellar contamination correction are unimportant beyond this magnitude. We have used our $J-K$ discriminator to eliminate stars more than 3 magnitudes brighter than the 5 σ limit of each cluster's K data, and then switch to the Bahcall & Soneira model predictions at fainter magnitudes. In the end, the stellar contamination amounts to only a few stars per half-magnitude bin in each cluster.

3.2. Galaxy Counts

We need to correct our cluster galaxy number counts for contamination by background and foreground galaxies. This is carried out statistically, using field galaxy counts from our own observations (Dickinson et al. 1999; EES) and the literature. Our primary source is the K–band photometry of EES, which has been carried out in exactly the same manner as for our clusters.

In Figure 4 we plot K counts from the EES survey, the Hubble Deep Field North (HDF–N) using the ground based IR imaging of Dickinson et al. (1999), and a selection of deep K counts from the literature. Error bars are calculated following the recipes of Huang et al. (1997) to include an extra contribution due to galaxy clustering. The agreement between the various data sets is generally good, within the variation expected from counting statistics. There is an excess in the HDF–N at $17<K<19$: comparison of the $J-K$ color distribution of these galaxies with objects of the same magnitude in EES shows no difference. We suggest that this excess is due to a random enhancement in the numbers of bright galaxies in the small HDF–N volume.

Next, we obtain linear fits to the $K<16$ and $K>18$ counts. For $K<16$ we derive a

slope of 0.677, in excellent agreement with the 0.689 of Huang et al. (1997). For $K > 18$ we find a slope of 0.302, steeper than the 0.261 of Huang et al. but in satisfactory agreement with other K–band counts (e.g., Moustakas et al. 1997). Finally, we correct for field galaxies using the $K < 16$ relation for objects at $K < 17$, and the $K > 18$ relation for fainter objects, normalized to the area observed in each cluster. Errors for these galaxy counts, used for background subtraction, are calculated according to the prescription of Huang et al. After subtracting stars and field galaxies, the remaining numbers of objects in each cluster, which are assumed to be member galaxies, are given in Table 1 in the column N_{memb}.

3.3. Luminosity Functions

We divide our sample of clusters into 10 redshift bins, with central z between 0.15 and 0.9 as listed in Table 2. Each bin includes typically four clusters, but this number varies from bin to bin. For example, there are only two clusters in each of the $z = 0.15$ and 0.25 bins and so the errors on the fitted K^* are relatively large. For each cluster we determine the appropriate magnitude intervals based on the difference between the cluster redshift and the midpoint redshift of each bin, including the small k–correction, so that the intervals will align at the midpoint redshift. For example, the $K = 16.25 - 16.75$ interval for the midpoint $z = 0.397$ bin corresponds to $K = 16.38 - 16.89$ for GHO 0303+1706 at $z = 0.418$. We then count the objects in the appropriate 0.5 magnitude intervals, removing stars from the brighter intervals using $J - K$ colors. Finally faint stars and field galaxies are removed by interpolating model counts to these intervals using the methods specified in §3.1 and §3.2. Errors in the raw cluster counts and in the star count models are assumed to be Poissonian, whereas for contaminating galaxies we add an extra contribution due to clustering, as in §3.2. We assume errors propagate in quadrature.

For each redshift bin, we sum number counts for all clusters in order to reduce shot noise and average over uncertainties in background subtraction. We fit the composite LF in each bin with a Schechter function, fixing the faint end slope to have $\alpha = -0.9$. This is the value measured in the infrared LF of the Coma cluster for $K < K^* + 3$ (De Propris et al. 1998) and also for the field (Gardner et al. 1997). We choose not to fit α because our photometry only reaches to $\sim$2 magnitudes below L^*. The optical LFs for bright cluster galaxies also have $\alpha \sim -1$, although there is considerable variation in the slope fainter than four magnitudes below L^*. We derive values for K^* and the associated errors using the maximum likelihood technique of Sandage, Tammann, & Yahil (1979). Luminosity functions for each of our redshift bins are shown in Figure 5. The derived values and their 1σ uncertainties are given in Table 2.

Finally, we have divided the sample in two ways in an attempt to ascertain the effects of cluster mass on $K^*(z)$. First, we separated by X-ray luminosity (Table 1) at $L_X \sim 4 \times 10^{44}$ ergs^{-1} s^{-1} (0.3–3.5 keV). This is close to the characteristic L_X^* of the X-ray luminosity function measured at similar redshifts (Rosati et al. 1998). X-ray data were available for 27 clusters from our sample; the remaining 11 were excluded from this analysis. X-ray luminosity correlates with total cluster mass, which may be the main parameter of interest for testing theoretical models of galaxy formation in clusters. Schechter functions were fit separately to the low– and high–L_X subsamples, again binned by redshift, with α fixed at -0.9. The fitted K^* are given in Table 3 and the LFs are shown in Figure 6.

We also divided the clusters on the basis of "member" surface density as a measure of the cluster richness. The statistical N_{memb} were normalized by the field size of the K-band images to calculate the near-IR cluster galaxy density. For this purpose, clusters were excluded for which our K-band images were relatively shallow compared to the other data at similar redshift. The excluded clusters are MS 1253.9+0456, Cl 2244-02, Abell 370, 3C 313, Vidal 14, and 3C 34. The remaining 32 clusters were divided at a "member" surface density of 85 Mpc^{-2} into rich and poor groupings. Again, Schechter functions were fit separately to the rich and poor subsamples binned by redshift, with α fixed at -0.9. The fitted K^* are given in Table 4 and the LFs are shown in Figure 7.

4. Discussion

The behavior of the characteristic magnitude K^* with redshift is shown in Figure 8, along with spectral synthesis models for no–evolution (i.e. pure k–correction) and passive evolution constructed using GISSEL (Bruzual & Charlot 1993, 1997; hereinafter BC). All galaxy models used in this paper form stars in a 0.1 Gyr burst with a Salpeter IMF and with solar metallicity. The models plotted in Figure 8 were normalized to $K^* = 10.9 \pm 0.2$ at the Coma cluster (De Propris et al. 1998), although this normalization was left free for the statistical tests described below. The no–evolution (NE) predictions use model spectra with ages of 10 Gyr for the $\Omega_M = 1$, $\Lambda = 0$ cosmology, 11 Gyr for $\Omega_M = 0.3$, $\Lambda = 0$, and 12 Gyr for $\Omega_M = 0.3$, $\Lambda = 0.7$. However, in the near infrared the spectra of galaxies vary so little that virtually any reasonable model spectrum yields very similar k–corrections.

The observed K^* vs. z relation is inconsistent with an unevolving luminosity function, especially for the low–Ω_M cosmologies. The measured K^* values become systematically brighter at higher redshifts relative to the NE models. We have tested our data against the three NE models, including the Coma K^* data point and allowing for free normalization of the absolute magnitude scaling. A simple least–squares fit gives the following values

for the reduced χ^2 (for 10 degrees of freedom): 3.0 for $\Omega_M = 1$, $\Lambda = 0$; 4.0 for $\Omega_M = 0.3$, $\Lambda = 0$; and 6.2 for $\Omega_M = 0.3$, $\Lambda = 0.7$. The formal probabilities of these models being consistent with the data are 8.8×10^{-4}, 1.6×10^{-5}, and 1.5×10^{-9}, respectively. The anticorrelation of absolute magnitude with redshift (i.e. luminosity evolution) was examined by applying the Spearman rank–order test to the difference between the data points and the NE models. This gives correlation coefficients of -0.83, -0.86 and -0.90 for the above three cosmologies. The probabilities that these anticorrelations would arise by chance from an unevolving data set are 8.4×10^{-4}, 4.0×10^{-4}, and 8.0×10^{-5}, respectively.

The passively evolving models were calculated for the $\Omega_M = 0.3$, $\Lambda = 0$ and $\Omega_M = 0.3$, $\Lambda = 0.7$ cosmologies, assuming $H_0 = 65$ km s^{-1} Mpc^{-1} and with formation redshifts $z_f = 2$ and 3. These provide a better fit to the data than do the NE models. We do not attempt to discriminate statistically between the different evolving models because the cosmological parameters, formation redshifts, and star formation histories can be traded off against one another to yield comparably good fits for different scenarios. For passively evolving models in the $\Lambda = 0.7$ cosmology, $z_f = 2$ provides a slightly better fit than does $z_f = 3$, while for $\Lambda = 0$ the $z_f = 3$ model is favored. Extending this analysis to clusters at $z > 1$ should help to distinguish between the different models.

Barger et al. (1998) presented K–band LFs for a sample of 10 clusters at $0.31 < z < 0.56$. Assuming a fixed $\alpha = -1.0$, $H_0 = 50$ km^{-1} s^{-1} Mpc^{-1}, and $q_0 = 0.5$, they found $M^*(K_{rest})$ of -25.41, -25.51, and -25.29 for their redshift bins at $z = 0.31, 0.40$, and 0.56, respectively. They claimed no significant luminosity evolution from a comparison of these values with the $M^*(K_{rest}) = -25.1$ determined by Mobasher et al. 1993 for a local *field* sample. However, the expected departure from no–evolution at $z = 0.56$, the highest redshift bin in Barger et al., is $\sim$0.5 mag in the observed K–band, which is only about twice the errors in their derived $M^*(K_{rest})$. If the Barger et al. values are compared with $M^*(K_{rest}) = -24.8 - 5 \log h_{50}$ which we have measured for the Coma cluster (De Propris et al. 1998), they are consistent with the amount of passive evolution that we observe. Another recent study of the K–band LF in distant clusters (Trentham & Mobasher 1998) appears to find no evolution, though this is difficult to discern because no Schechter function fits were made, and their data covered small areas in only 5 clusters. By fitting infrared LFs using a uniform data set that spans a very wide range of redshifts, we have measured evolution within a single cluster sample without requiring comparisons to measurements from other published samples which were observed and analyzed in a different way.

Our key result is the consistency between the observed evolution of the infrared *luminosities* of cluster galaxies and their *color* evolution as manifested by the slope, scatter and intercept of the color–magnitude relation (Aragón-Salamanca et al. 1993; SED95;

SED98; Ellis et al. 1997). Both are fully consistent with simple, passive spectrophotometric evolution of a galaxy population which has been largely stable throughout the redshift range $0 < z < 1$. Kauffmann & Charlot (1998a) have shown that the apparently passive evolution of the color–magnitude relation can be accommodated within a hierarchical model, even if the galaxies themselves still grow by mergers until late times. Our new measurements show that galaxies in high redshift clusters also follow the same intrinsic luminosity distribution as do those today, once passive evolution is taken into account, strongly suggesting that their bulk stellar masses have not increased substantially since $z = 1$. It is interesting to note that Aragón–Salamanca et al. (1998) find that the *brightest* cluster galaxies (BCGs) exhibit a rather different behavior, with infrared luminosities which are *fainter* at high redshift once the expected evolution of their stellar populations is taken into account. They interpret this as evidence that BCGs have grown with time by accretion, a behavior which we would suggest is not shared by the bulk of the cluster population.

Previous photometric studies of early–type cluster galaxies at other wavelengths have reached conclusions that are qualitatively similar to our own. The rest frame B–band surface brightnesses of cluster ellipticals at $z \leq 1.2$ have been shown to be consistent with high-z formation and passive evolution (Dickinson 1995, 1997; Pahre, Djorgovski & De Carvalho 1996; Schade, Barrientos & Lopez-Cruz 1997; Barger et al. 1998), albeit with large uncertainties. Moreover, recent studies exploiting the full power of the Fundamental Plane now probe nearly the same redshift range as do our LFs (e.g. Kelson et al. 1997; van Dokkum et al. 1998). These have shown that the rest–frame B–band mass–to–light ratio (M/L) of early–type cluster galaxies evolved in a manner consistent with passive luminosity evolution. Early results derived from a small sample at $z = 0.83$ indicate a limit on the formation redshift for cluster ellipticals of $z_f > 1.7$ in an $\Omega_M = 0.3$, $\Omega_\Lambda = 0.7$ universe (van Dokkum et al. 1998). If the evolution of both M/L and of the luminosity function can be consistently explained by passive stellar evolution, then it would follow that the *mass function* of cluster galaxies is approximately invariant over the range of redshifts and luminosities which have been studied to date.

The luminosity evolution that we observe in our cluster sample is strikingly different from that which has been reported for *field* galaxy samples, particularly those selected in the near–infrared or limited to early–type galaxies only. Cowie et al. (1996) present rest–frame K–band luminosity functions derived from a field galaxy sample spanning $0 < z < 1.6$, and find that L_K^* remains constant or declines at higher redshifts. Similarly, Kauffmann, Charlot, & White (1996) cite evidence for a strong negative luminosity evolution of early–type field galaxies selected by color from the Canada–France Redshift Survey (Lilly et al. 1995a). Kauffmann & Charlot (1998b) have highlighted the deficit of high redshift galaxies at $K < 19$ in the infrared–selected surveys of Songaila et al. (1994) and Cowie et

al. (1996).

This apparent deficit of bright, high redshift field galaxies has been cited as evidence supporting hierarchical models which would assemble the most massive galaxies at relatively late epochs. This interpretation is not necessarily inconsistent with our measurements, since field and cluster galaxies may follow different evolutionary histories. Indeed, in the semi–analytic models of Kauffmann & Charlot (1998a), cluster ellipticals form earlier than field ellipticals, and might therefore be expected to show different luminosity evolution. At some level, if the assembly of galaxies is pushed back to higher redshifts in denser environments, then it is inevitable that their subsequent behavior will more closely resemble passive evolution at late times, and the distinction between "passive" and "hierarchical" models will blur.

There is conflicting evidence on the question of the dependence of elliptical galaxy evolution on environment. Schade et al. (1996) find no difference in the M_B-$\log r_e$ relations of distant field and cluster ellipticals. Bernardi et al. (1998) find nearly identical Mg_2-σ relations for field and cluster ellipticals from large, nearby galaxy samples, and use this to limit mean age differences to be < 1 Gyr, arguing that the bulk of stars in galactic spheroids was formed at high redshift, independent of environmental density. This is also the conclusion reached by De Propris et al. (1998) on the basis of the very similar infrared luminosity functions of field and cluster galaxies. On the other hand, Worthey and collaborators (e.g., Worthey 1997 and references therein) have suggested that field E/S0 galaxies span a large range of ages, on the basis of Balmer line strengths in their integrated spectra. This is not necessarily inconsistent with our findings, since relatively small bursts suffice to account for the observations. Conversely, far-ultraviolet components may significantly affect the use of narrow band spectral indices as age indicators (Davies, Sadler, & Peletier 1993).

Kauffmann & Charlot (1998a) suggest that studies of galaxies in rich clusters are strongly biased, as they select massive objects whose members are likely to have formed at high redshift in any scenario for structure formation. They argue that the evidence for passive evolution comes from selecting samples which are most likely to be passively evolving. Our sample includes clusters which span two orders of magnitude in X-ray luminosity, with a wide range of optical richness, and presumably also of mass. As described in §3.3, we have divided our cluster data into subsamples with high and low X-ray luminosity, and with rich and poor "member" density, in order to test whether the luminosity evolution depends on the mass and/or optical richness of the cluster. The behavior of K^* vs. z for the two X-ray subsamples (Figure 9) and for the rich vs poor groupings (Figure 10) appear to be similar in each case. The only exception is in the highest

redshift bin in the rich vs poor comparisons, where K^* for the rich clusters is brighter than that of the poor clusters at about the 2σ level. Overall, these two methods both indicate that the luminosity evolution of massive galaxies is similar across the range of cluster environments spanned by our sample, and that biases of the type suggested by Kauffmann & Charlot (1998a) are likely to be weak, at least for environments richer than groups.

The LFs presented here sum the entire population of galaxies within a radius of $\sim$0.5 to 1 Mpc from the cluster centers. For $K < K^* + 2$, this is likely to be dominated by E/S0 galaxies and early type spirals, although the morphology–density and morphology–radius relationships appear to be weaker in clusters at high redshift (Dressler et al. 1997). It is unclear how the changing morphological mix of galaxies in distant clusters might affect the K–band luminosity functions, but the presence of an increasingly numerous population of blue, star–forming cluster galaxies at higher redshifts does not fit well within any simple model of pure, passive evolution. Since the infrared LF primarily measures the distribution of stellar mass among galaxies, the apparently passive luminosity evolution and "active" Butcher–Oemler population might be reconciled if the starbursts involve only a small fraction of the total mass in each galaxy. Indeed, population synthesis models show that even relatively small amounts of star formation, in terms of the total stellar mass fraction, can account for the colors of most blue galaxies in distant clusters (Barger et al. 1996).

5. Conclusions

We have presented K–band luminosity functions for a heterogeneous sample of 38 galaxy clusters spread over $0.1 < z < 1$. Schechter function fits to the field–corrected galaxy counts yield K^* values brighter than would be expected for a non–evolving population of early–type galaxies at $z > 0.4$ in low Ω cosmologies, and consistent with pure, passive luminosity evolution. This result supports and extends our previous results based on analysis of the color evolution of early–type cluster galaxies over the same redshift range. The positive luminosity evolution for cluster galaxies appears to differ from the flat or negative evolution which has been reported for infrared– and color–selected *field* galaxy samples out to $z \approx 1$ (Cowie et al. 1996; Kauffmann, Charlot & White 1996; Kauffmann & Charlot 1998b), perhaps suggesting a different evolutionary history for massive galaxies in different environments. However, we do not observe different evolution when we divide our cluster sample by X-ray luminosity or by richness.

These observations point to the importance of obtaining a census of galaxy properties over a wide range of environments for understanding the mechanisms which drive galaxy evolution. Hierarchical models in which collisionless dark matter dominates galaxy dynamics

and evolution generally postulate that the formation of massive galaxies, such as cluster ellipticals, takes place by accretion and mergers that continue to low redshift. Our results indicate that the stellar populations of massive galaxies ($K < K^* + 2$) in cluster cores form at relatively high redshifts, $z \gtrsim 2$, and suggest that the assembly of those galaxies is largely complete by $z \sim 1$.

The authors would like to thank NOAO for a generous allocation of observing time to this project, and the staffs at Kitt Peak and Cerro Tololo for their help with the observing. This research has made use of the NASA/IPAC Extragalactic Database (NED) which is operated by the Jet Propulsion Laboratory, California Institute of Technology, under contract with the National Aeronautics and Space Administration. Support for this work was provided by NASA through grant number AR–5790.02–94A from the Space Telescope Science Institute, which is operated by the Association of Universities for Research in Astronomy, Inc., under NASA contract NAS5-26555. Funding for OSIRIS was provided by grants from The Ohio State University and National Science Foundation grants AST–9016112 and AST–9218449. Portions of the research described here were carried out by the Jet Propulsion Laboratory, California Institute of Technology, under a contract with NASA. Work performed at the Lawrence Livermore National Laboratory is supported by the DOE under contract W7405-ENG-48. Work at the University of New South Wales is supported by a grant from the Australian Research Council. We would like to thank an anonymous referee for a number of helpful suggestions.

REFERENCES

Aragón-Salamanca, A., Ellis, R.S., Couch,, W.J., & Carter, D., 1993, MNRAS, 262, 764

Aragón-Salamanca, A., Baugh, C.M., & Kauffmann, G., 1998, MNRAS, 297, 427

Arimoto, N. & Yoshii, Y. 1987, A&A, 173, 23

Bahcall, J.N. & Soneira, R.M. 1980, ApJS, 44, 73

Bahcall, J.N. & Soneira, R.M. 1981, ApJS, 47, 357

Barger, A.J. Aragón-Salamanca, A., Ellis, R.S., Couch,, W.J., Smail, I., & Sharples, R. 1996, MNRAS, 279, 1

Barger, A.J. et al. 1998, ApJ, 501, 522

Bender, R., Burstein, D., & Faber, S.M. 1993, ApJ, 411, 153

Bernardi, M. et al. 1998, ApJ, 508, L143

Bershady, M., Lowenthal, J.D., & Koo, D. 1998, ApJ, 505,50

Binggeli, B., Sandage, A., & Tammann, G.A. 1988, ARA&A, 26, 509

Bothun, G. D. & Gregg, M. J. 1990, ApJ, 350, 73

Bower, R.G., Lucey, J.R., & Ellis, R.S. 1992, MNRAS, 254, 589

Bruzual, G. & Charlot, S. 1993, ApJ, 405, 538

Bruzual, G. & Charlot, S. 1997, personal communication

Burstein, D. & Heiles, C. 1982, AJ, 87, 1165

Butcher, H.R. & Oemler, A. 1984, ApJ, 285, 426

Cole, S., Aragón-Salamanca, A., Frenk, C.S., Navarro, J.F., & Zepf, S.E. 1994, MNRAS, 271, 781

Couch, W.J., Sharples, R.M. 1987, MNRAS, 229, 423

Couch, W.J., Barger, A.J., Smail, I., Ellis, R.S. & Sharples, R.M. 1998, ApJ, 497, 188

Cowie, L.L., Gardner, J.P. & Wainscoat, R.J. 1993, ApJ, 415, L9

Cowie, L.L., Songaila, A., Hu, E.M., & Cohen, J.G. 1996, AJ, 112, 839

Davies, R. L., Sadler, E. M. & Peletier, R. F. 1993, MNRAS, 262, 650

De Propris, R., Eisenhardt, P.R., Stanford, S.A. & Dickinson, M. 1998 ApJ, 503, L45

De Propris, R., Eisenhardt, P.R., Stanford, S.A. & Dickinson, M. 1999, in preparation

Dickinson, M., 1995, in *Fresh Views of Elliptical Galaxies,* eds. A. Buzzoni, A. Renzini & A. Serrano (ASP: San Francisco), p. 283

Dickinson, M., 1997, in *Galaxy Scaling Relations: Origins, Evolution & Applications,* eds. L. da Costa & A. Renzini (Springer–Verlag), p. 215

Dickinson, M. et al. 1999, in preparation

Djorgovski, S. et al. 1995, ApJ, 438, L13

Dressler, A., Oemler, A., Butcher, H. & Gunn, J. E., 1994, ApJ, 430, 107

Dressler, A., Oemler, A., Couch, W.J., Smail, I., Ellis, R.S., Barger, A., Butcher, H., Poggianti, B.M., & Sharples, R.M., 1997, ApJ, 490, 577

Eggen, O.J., Lynden-Bell, D., & Sandage, A., 1962, ApJ, 136, 748

Ellis, R.S., Colless, M., Broadhurst, T., Heyl, J. & Glazebrook, K., 1996, MNRAS, 280, 235

Ellis, R.S., Smail, I., Dressler, A., Couch, W.J., Oemler, A., Butcher, H., & Sharples, R.M. 1997, ApJ, 483, 582

Elston, R., Eisenhardt, P.R., & Stanford, S.A. 1999, in preparation

Gardner, J.P., Sharples, R.M., Frenk, C.S. & Carrasco, B.E. 1997, ApJ, 480, L99

Gavazzi, G., Pierini, D., Boselli, A. 1996, A&A, 312, 397

Huang, J.S., Cowie, L.L., Gardner, J.P., Hu, E.M., Songaila, A. & Wainscoat, R. J. 1997, ApJ, 476, 12

Jørgensen, I. 1999, MNRAS, in press

Kauffmann, G., Charlot, S., & White, S.D.M. 1996, MNRAS, 283, L117

Kauffmann, G. & Charlot, S. 1998a, MNRAS, 294, 705

Kauffmann, G. & Charlot, S. 1998b, MNRAS, 297, L23

Kelson, D., van Dokkum, P. G., Franx, M., Illingworth, G. D. & Fabricant, D. 1997, ApJ, 478, L13

Kuntschner, H.L. & Davies, J.I. 1998, MNRAS, 295, L29

Leggett, S. K. 1992, ApJS, 82, 351

Lilly, S.J., Le Fevre, O., Crampton, D., Hammer, F. & Tresse, L. 1995a, ApJ, 455, 50

Lilly, S.J., Tresse, L., Hammer, F., Crampton, D., & Le Fèvre, O., L. 1995b, ApJ, 455, 108

Lubin, L. 1996, AJ, 112, 23

Madau, P., Pozzetti, L., & Dickinson, M.E. 1998, ApJ, 498, 106

Mamon, G.A. & Soneira, R.M. 1982, ApJ, 255, 181

Mathis, J. M. 1990, ARA&A, 28, 37

McLeod, B.A., Bernstein, G.M., Rieke, M.J., Tollestrup, E.V., & Fazio, G.G. 1995, ApJS, 96, 117

Moustakas, L.A., Davis, M., Graham, J.R., Silk, J., Peterson, B.A., & Yoshii, Y. 1997, ApJ, 475, 445

Pahre, M., Djorgovski, S.G., & De Carvalho, R.R., 1996, ApJ, 456, L79

Pahre, M., De Carvalho, R.R., & Djorgovski, S.G. 1998, AJ, 116, 1606

Perlmutter, S. et al. 1998, astro-ph 9812133

Poggianti, B.M. 1997, A&AS, 122, 399

Riess, A. et al. 1998, AJ, 116, 1009

Rosati, P. Della Ceca, R., Norman, C. & Giacconi, R. 1998, ApJ, 492, L21

Sandage, A., Tammann, G.A., & Yahil, A. 1979, ApJ, 232, 352

Schade, D., Carlberg, R., Yee, H. K. C., Lopez-Cruz, O. & Ellingson, E. 1996, ApJ, 464, L63

Schade, D., Barrientos, F. & Lopez-Cruz, O. 1997, ApJ, 477, L17

Schechter, P.L., 1976, ApJ, 203, 297

Songaila, A., Cowie, L.L., Hu, E.M.. & Gardner, J.P. 1994, ApJS, 94, 461

Stanford, S.A., Eisenhardt, P.R., & Dickinson, M. 1995, ApJ, 450, 512

Stanford, S.A., Eisenhardt, P.R., & Dickinson, M. 1998, ApJ, 492, 461

Trentham, N. & Mobasher, B. 1998, MNRAS, 299, 488

Valdes, F. 1982, in *Instrumentation in Astronomy IV*; Proceedings of the Fourth Conference, Bellingham, WA, SPIE, p. 465

van Dokkum, P., Franx, M., Kelson, D. & Illingworth, G. D. 1998, ApJ, 504, L17

Worthey, G., Trager, S., & Faber, S. 1996, in ASP Conference Series 86, *Fresh Views of Elliptical Galaxies*, eds. A. Buzzoni & Renzini, A. (San Francisco: ASP), 203

Worthey, G. 1997, in *Star Formation, Near and Far*, AIP Conference Series, vol.393; ed. by Steven S. Holt and Lee G. Mundy (Woodbury: AIP press), p. 525

This preprint was prepared with the AAS LaTeX macros v4.0.

Table 1. Cluster Sample

Name	R.A. J2000	Dec. J2000	Data[a]	Field arcmin^2	z	K_{lim} mag	N_{samp}	N^b_{memb}	L_x 10^{45} ergs/s
Abell 1146	11:01:20.6	−22:43:08	4	59.3	0.142	16.5	187	129	0.33
Abell 3305	05:01:52.9	−39:12:45	4	52.9	0.157	16.5	100	46	···
MS 0906.5+1110	09:09:16.7	+10:58:38	4	57.5	0.180	16.9	207	146	0.57
Abell 1689	13:11:34.2	−01:21:56	4	54.1	0.182	17.4	259	176	1.30
Abell 1942	14:38:37.0	+03:40:05	4	15.9	0.224	17.5	121	96	0.16
MS 1253.9+0456	12:56:28.8	+04:40:02	4	16.1	0.230	17.2	117	94	0.52
Abell 1525	12:22:03.8	−01:08:38	4	16.0	0.259	17.5	85	55	···
MS 1008.1-1224	10:10:34.1	−12:39:48	4	17.2	0.301	17.9	207	154	0.43
MS 1147.3+1103	11:49:55.7	+10:46:37	4	14.9	0.303	17.9	115	79	0.38
AC 118	00:14:19.3	−30:23:18	3	24.4	0.308	18.5	292	200	1.60
AC 103	20:57:07.5	−64:38:53	3	23.8	0.311	18.2	277	203	···
AC 114	22:58:52.0	−34:46:54	3	21.8	0.312	18.3	276	161	0.50
MS 2137.3-234	21:40:14.5	−23:39:41	3	24.3	0.313	18.1	184	135	1.50
Abell S0506	05:01:04.0	−24:24:42	4	18.4	0.316	18.0	150	92	0.13
MS 1358.1+6245	13:59:54.3	+62:30:36	1	21.5	0.328	18.2	179	116	1.06
Cl 2244-02	22:47:12.9	−02:05:40	1	21.5	0.330	18.8	213	114	0.50
Abell 370	02:39:53.8	−01:34:24	5	22.4	0.374	18.1	190	145	1.10
Cl 0024+16	00:26:35.4	+17:09:51	1	21.4	0.391	18.8	329	230	0.22
Abell 851	09:43:02.6	+46:58:37	5	21.5	0.405	18.7	306	196	0.80
GHO 0303+1706	03:06:15.9	+17:19:17	1	21.3	0.418	18.8	252	186	0.22
3C 313	15:10:59.6	+07:51:49	1	21.3	0.461	18.5	158	60	···
3C 295	14:11:19.5	+52:12:21	1	21.9	0.461	18.8	222	133	···

Table 1—Continued

Name	R.A. J2000	Dec. J2000	Data[a]	Field arcmin^2	z	K_{lim} mag	N_{samp}	N^b_{memb}	L_x 10^{45} ergs/s
F1557.19TC	04:12:51.6	−65:50:17	3	24.1	0.510	19.1	231	131	0.05
Vidal 14	00:49:11.1	−24:40:55	3	22.1	0.520	18.0	143	90	···
GHO 1601+4253	16:03:10.6	+42:45:35	1	21.6	0.539	19.2	264	165	0.14
MS 0451.6-0306	04:54:10.8	−03:00:57	2	6.6	0.539	19.2	153	110	1.90
Cl 0016+16	00:18:33.6	+16:25:46	1	21.7	0.545	19.1	338	241	1.60
J1888.16CL	00:56:54.6	−27:40:31	3	21.1	0.560	19.2	253	156	0.12
MS 2053.7-0449	20:56:22.4	−04:37:43	3	27.7	0.582	19.2	443	215	0.56
GHO 0317+1521	03:20:02.3	+15:31:49	2	7.4	0.583	19.2	72	7	···
3C 220.1	09:32:39.6	+79:06:32	1	20.2	0.620	19.5	245	209	···
GHO 2201+0258	22:04:05.7	+03:12:50	2	8.1	0.640	19.3	93	31	···
3C 34	01:10:18.5	+31:47:20	2	6.5	0.689	19.1	156	109	···
GHO 1322+3027	13:24:49.3	+30:11:28	2	6.5	0.751	20.3	163	112	0.09
MS 1137.5+6625	11:40:23.3	+66:08:41	2	7.1	0.782	20.0	135	48	0.75
MS 1054.5-032	10:56:59.5	−03:37:28	2	6.5	0.828	20.3	201	160	0.90
GHO 1603+4313	16:04:18.9	+43:04:36	2	6.9	0.895	20.3	144	59	0.12
GHO 1603+4329	16:04:31.5	+43:21:17	2	7.2	0.920	20.1	150	59	···

[a]1 = KPNO 2.1m and IRIM; 2 = KPNO 4m and IRIM; 3 = CTIO 1.5m and CIRIM; 4 = CTIO 1.5m and OSIRIS; 5 = KPNO 1.3m and SQIID

[b]Number of cluster "members" left, in a statistical sense, after removing contaminating stars and galaxies following the methods outlined in §3

Table 2. K^* vs. z for the complete cluster sample

Redshift	K^*	Clusters/bin
0.15	14.84 ± 0.49	2
0.20	15.16 ± 0.07	3
0.25	15.64 ± 0.38	2
0.32	15.74 ± 0.08	9
0.40	16.50 ± 0.11	4
0.46	16.38 ± 0.08	2
0.54	16.85 ± 0.18	6
0.61	17.57 ± 0.41	4
0.79	17.51 ± 0.26	4
0.90	18.05 ± 0.25	2

Table 3. K^* vs. z for high and low X–ray luminosity subsamples

Redshift	K^*(high L_X)	Clusters/bin	K^*(low L_X)	Clusters/bin
0.20	15.15 ± 0.22	3	15.08 ± 0.15	2
0.32	15.64 ± 0.12	5	15.89 ± 0.27	3
0.40	15.77 ± 0.28	2	16.09 ± 0.14	2
0.54	16.81 ± 0.15	3	16.88 ± 0.22	3
0.83	17.64 ± 0.31	2	17.93 ± 0.10	2

Table 4. K^* vs. z for rich and poor subsamples

Redshift	K^*(rich)	Clusters/bin	K^*(poor)	Clusters/bin
0.20	15.00 ± 0.11	3	15.25 ± 0.41	2
0.32	15.77 ± 0.16	4	15.53 ± 0.11	6
0.40	16.03 ± 0.16	2	16.28 ± 0.13	2
0.54	16.75 ± 0.18	2	16.50 ± 0.22	6
0.83	17.21 ± 0.28	2	18.05 ± 0.25	3

Fig. 1.— Redshift distribution of the clusters used in the luminosity function analysis.

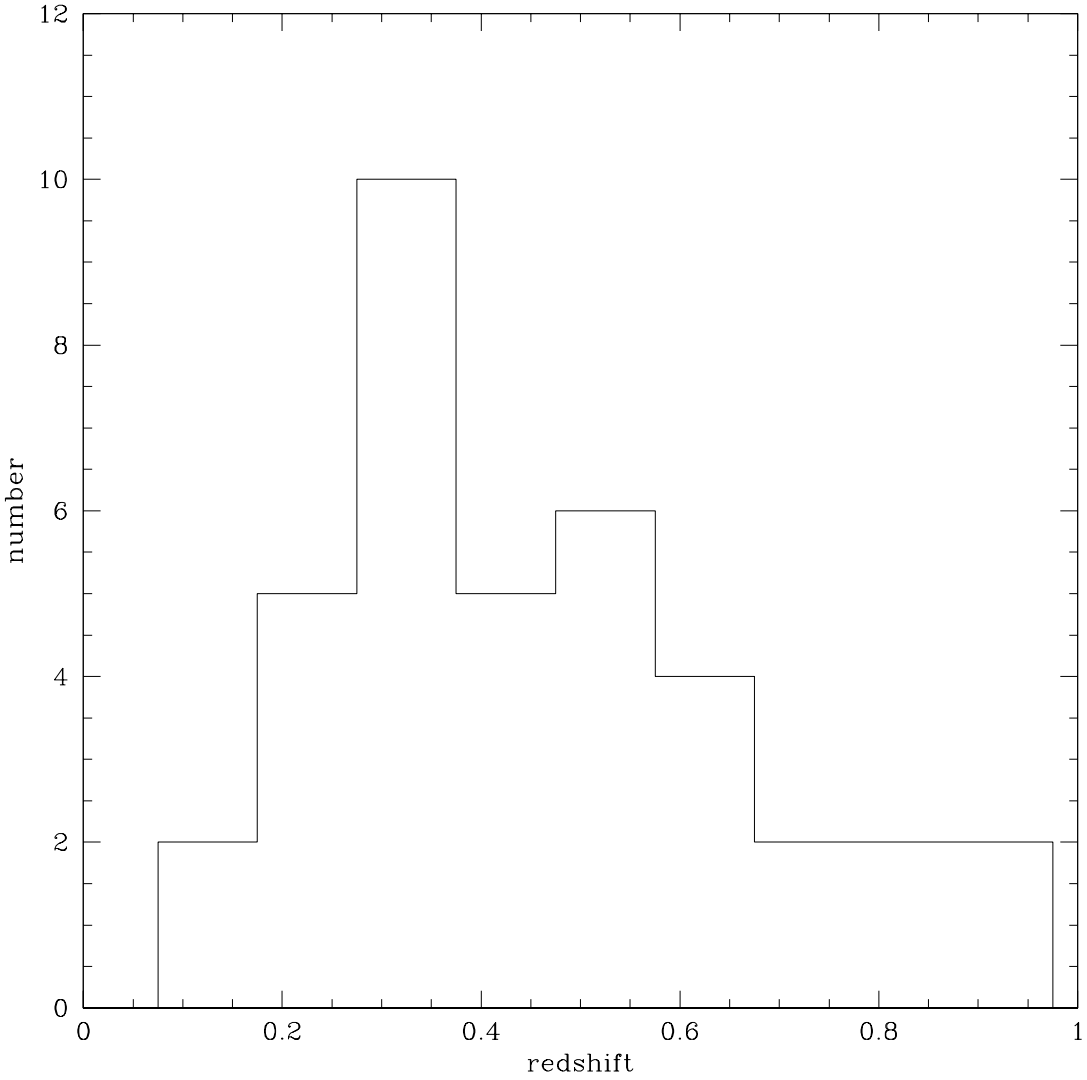

Fig. 2.— Color–magnitude diagram for objects in a subset of the clusters with *HST* imaging. Filled squares are stars, and open circles are galaxies, as determined from archival WFPC2 images. A $J - K = 1$ line effectively separates stars and galaxies.

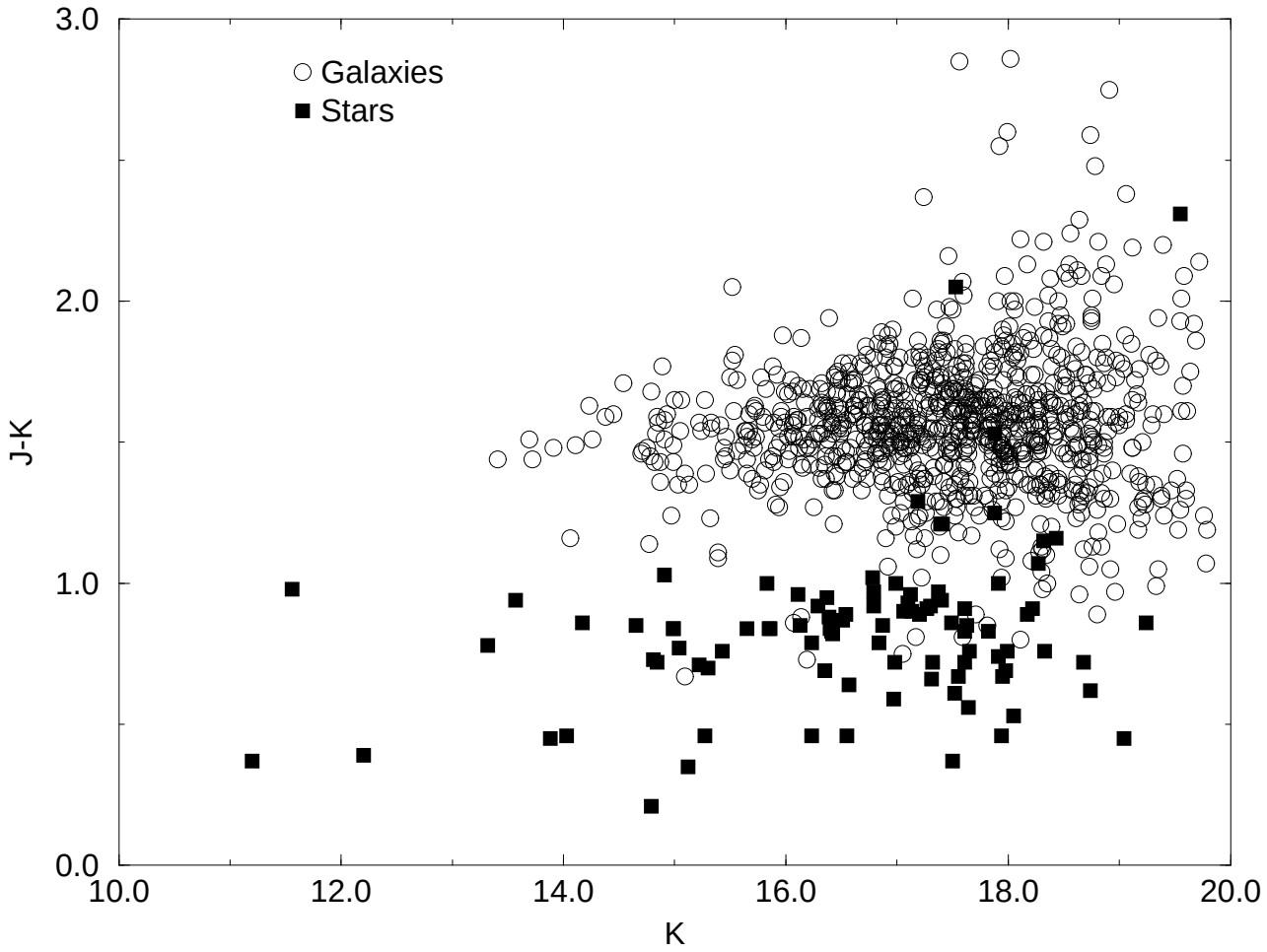

Fig. 3.— Star counts in the four ∼25 arcmin^2 fields observed fby Elston et al. (1999), selected using the color criterion of Huang et al. 1997 (open squares), and with our $J - K$ criterion (filled circles). The thick solid lines show predictions from the the models of Bahcall & Soneira (1980, 1981).

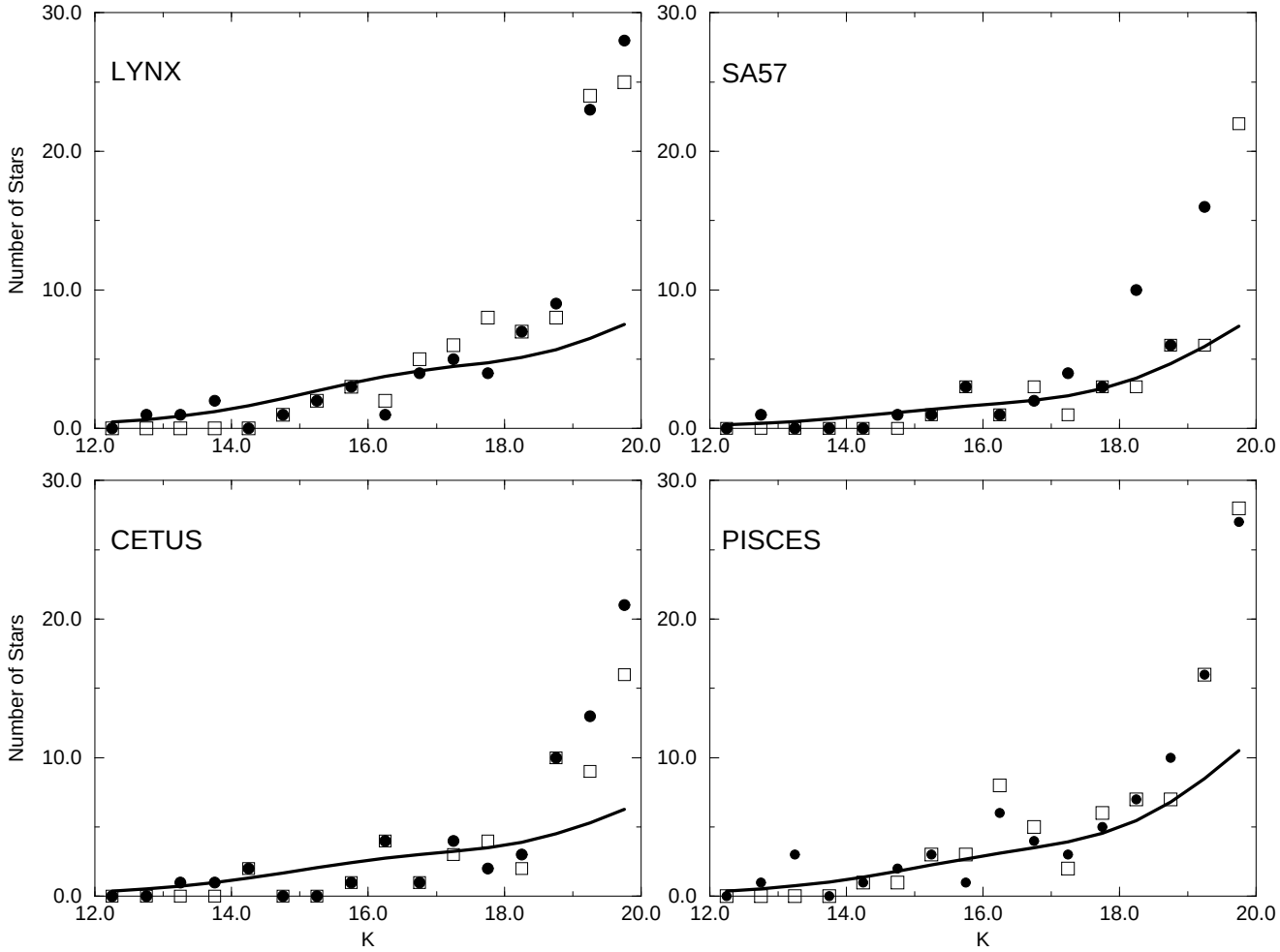

Fig. 4.— K–band galaxy counts from near-IR field surveys (Dickinson et al. 1999 and Elston et al. 1999 – filled symbols) and from the literature: the HWS, HMWS and HMDS are from Cowie et al. (1993).

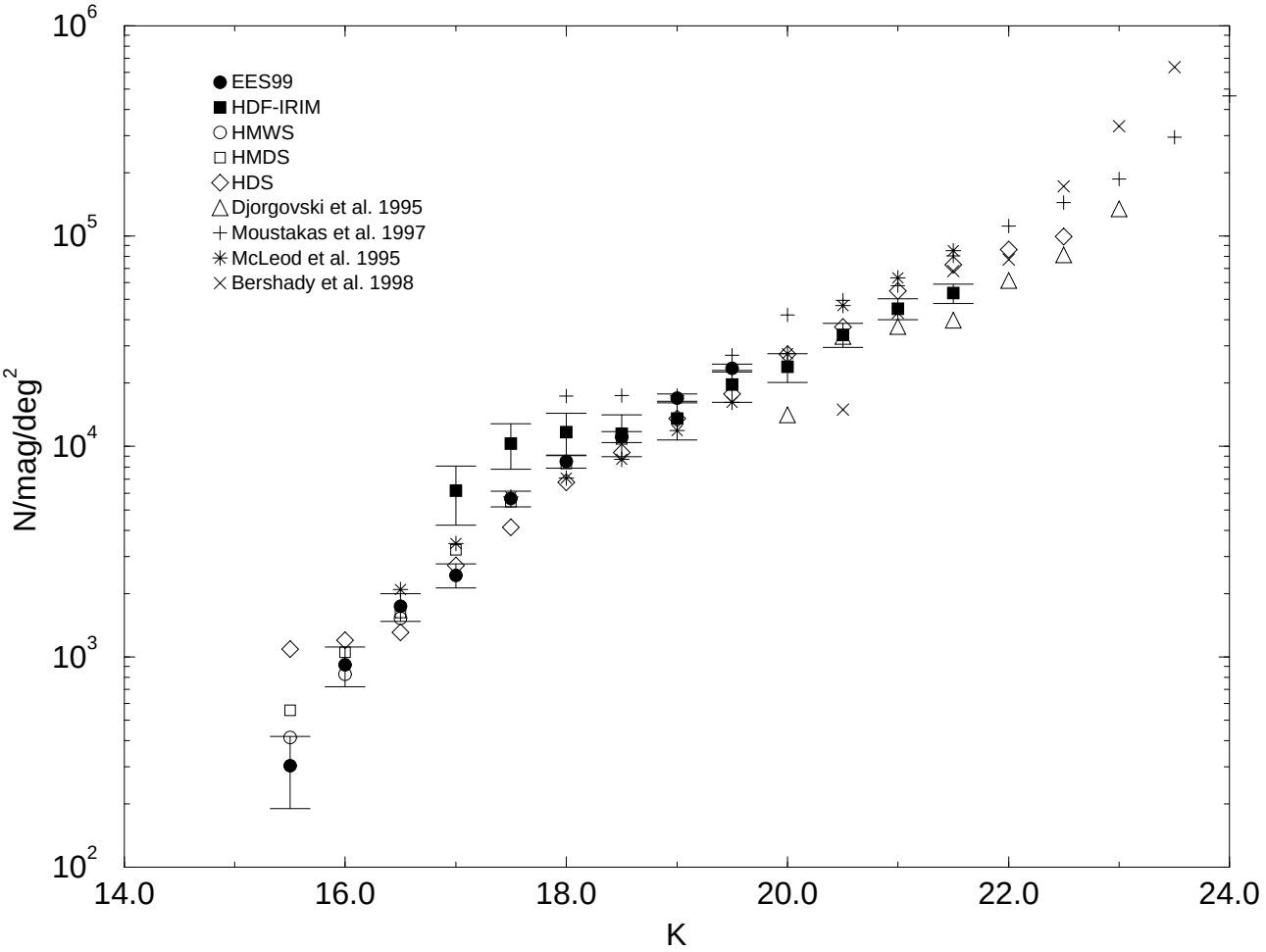

Fig. 5.— Cumulative K–band luminosity functions for all redshift bins. Solid lines are the Schechter function fits with $\alpha = -0.9$.

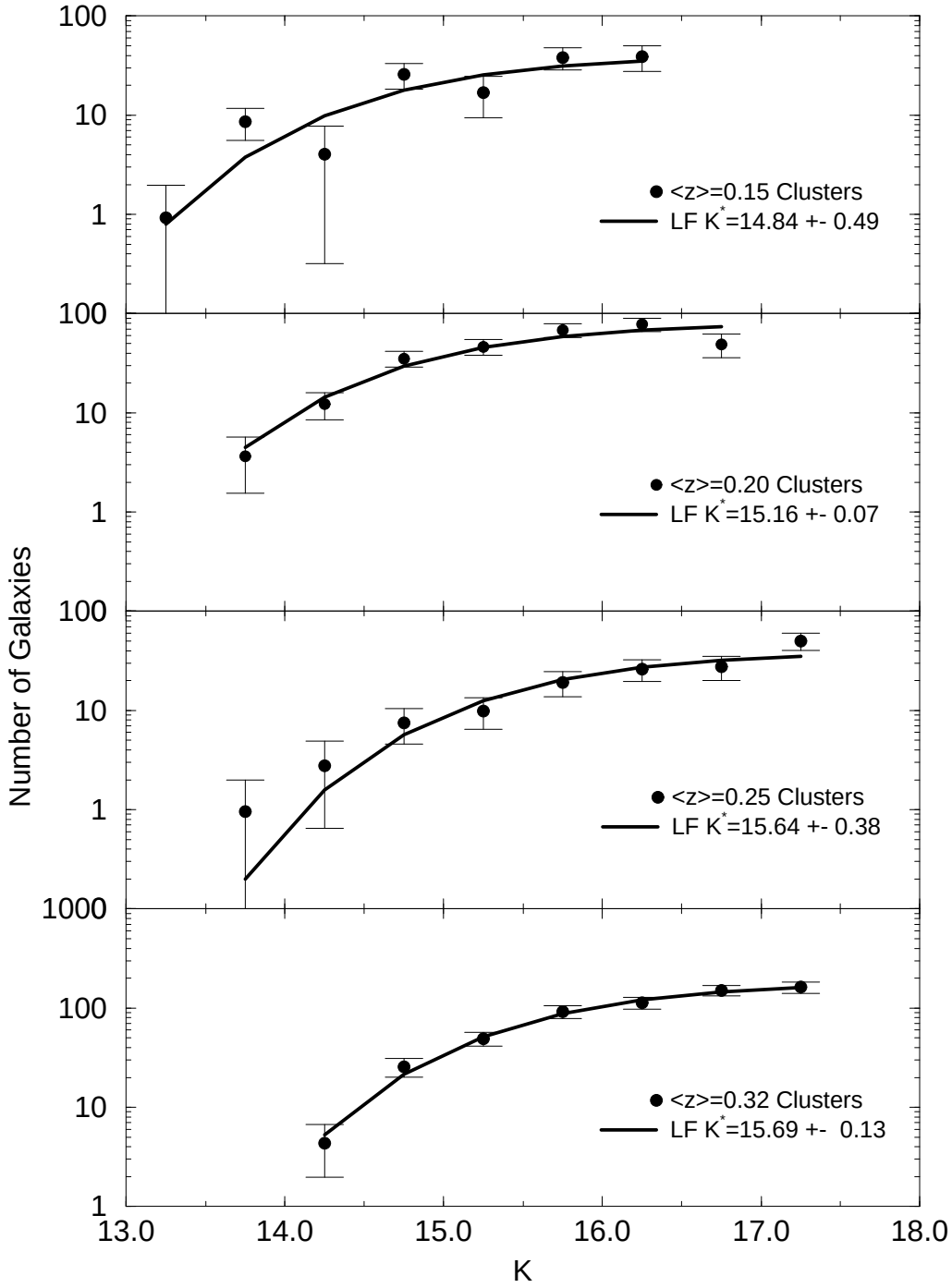

Fig. 5.— (continued)

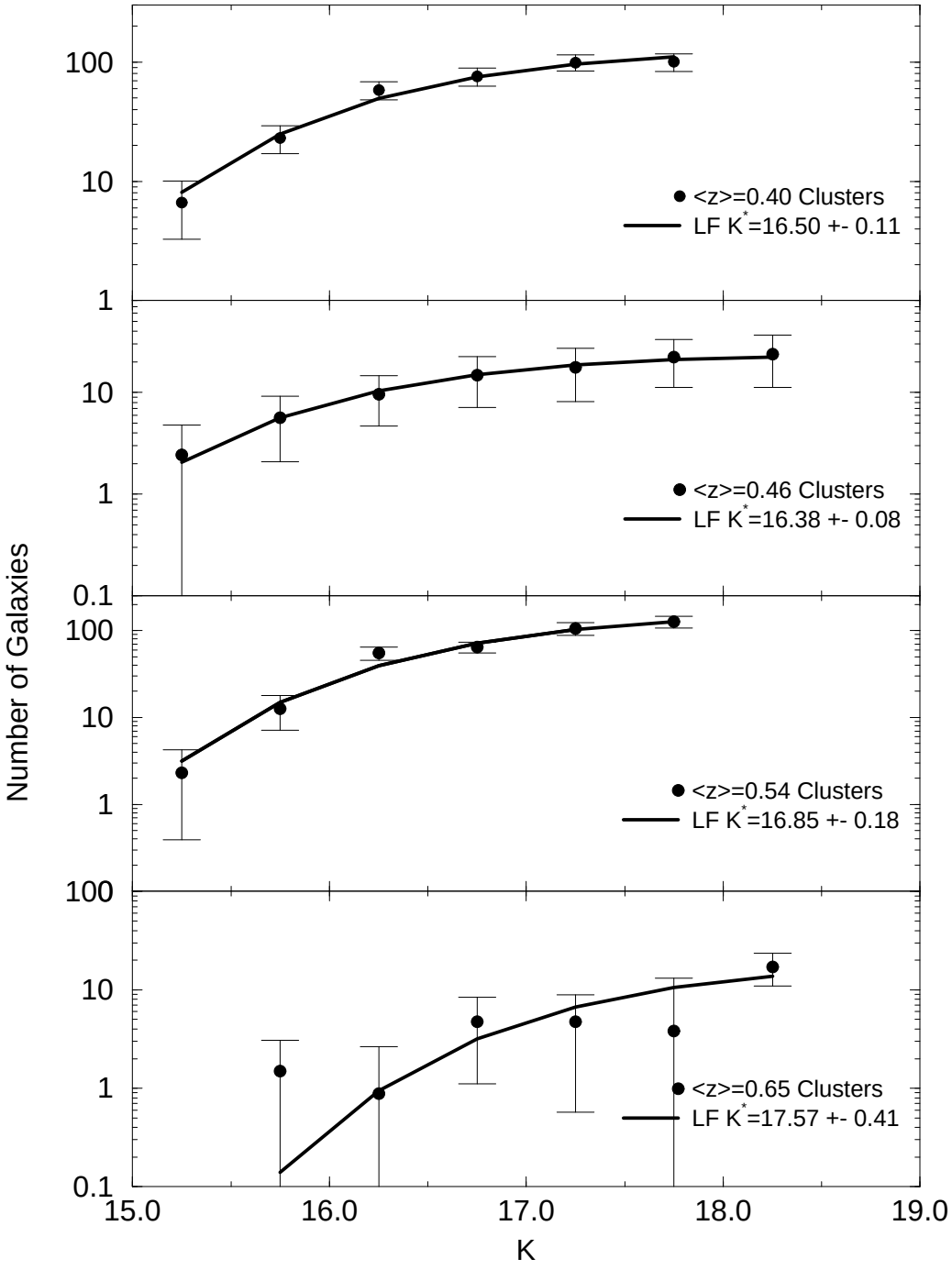

Fig. 5.— (continued)

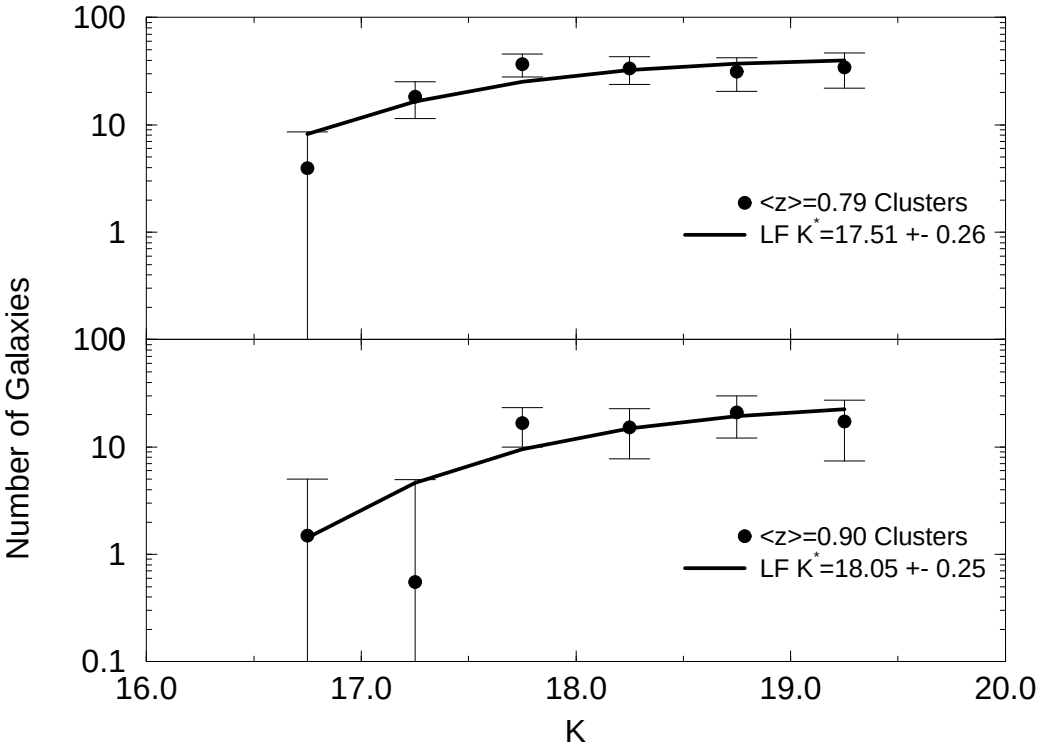

Fig. 6.— Cumulative luminosity functions in five redshift bins for high and low X-ray luminosity cluster subsamples, chosen as described in the text. The solid and dashed lines are the Schechter function fits with $\alpha = -0.9$.

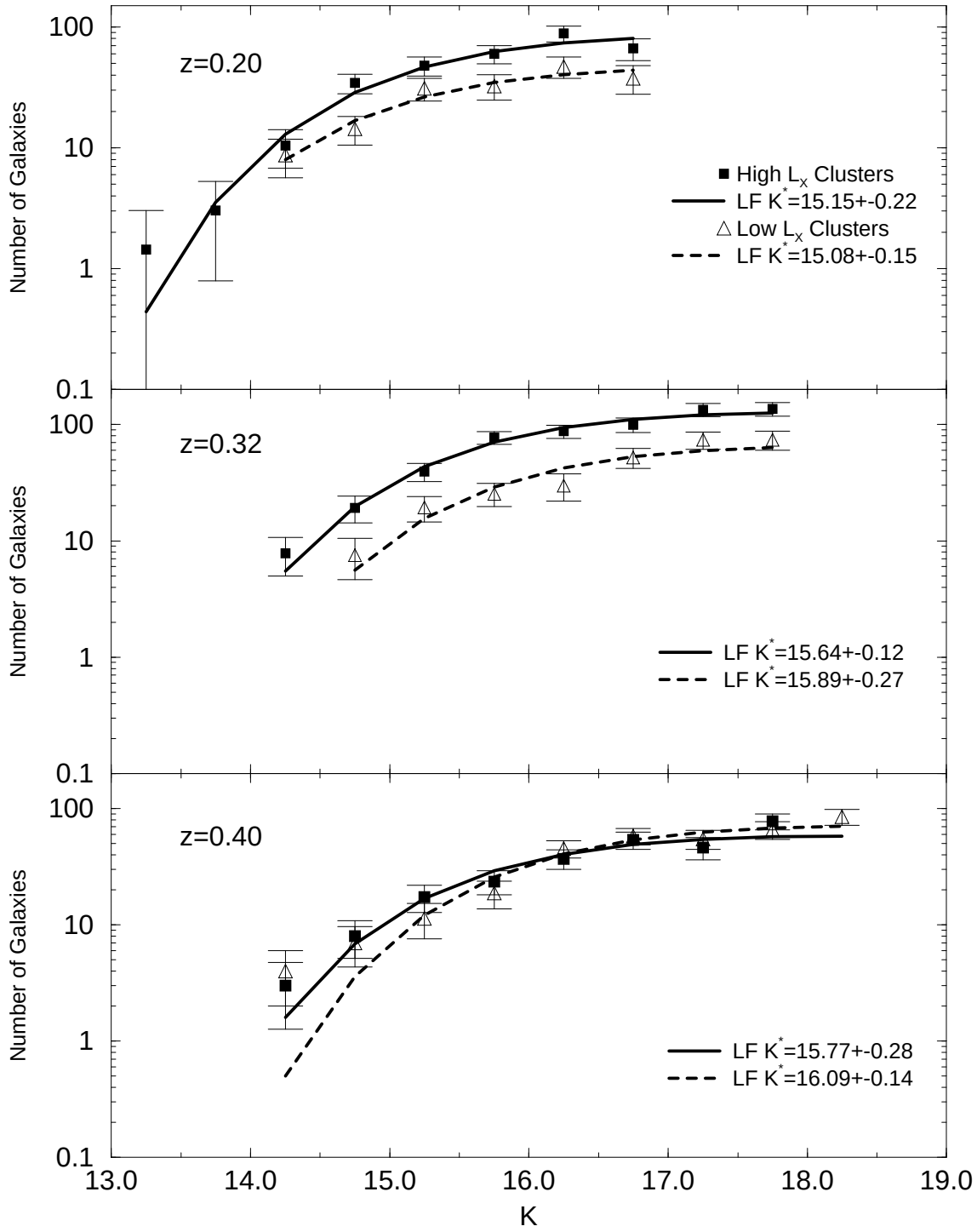

Fig. 6.— (continued)

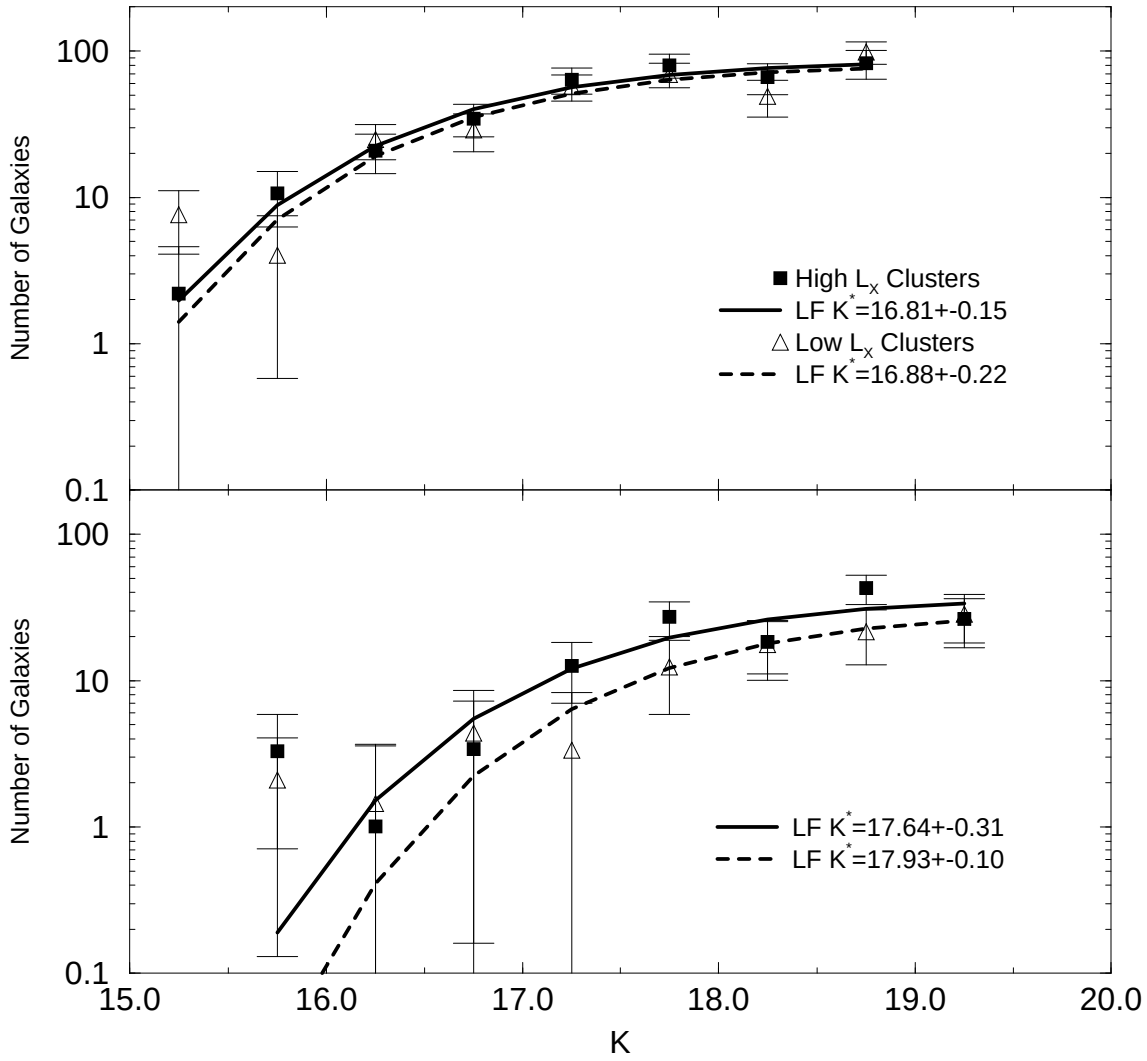

Fig. 7.— Cumulative luminosity functions in five redshift bins for the rich and poor cluster subsamples, chosen as described in the text. The solid and dashed lines are the Schechter function fits with $\alpha = -0.9$.

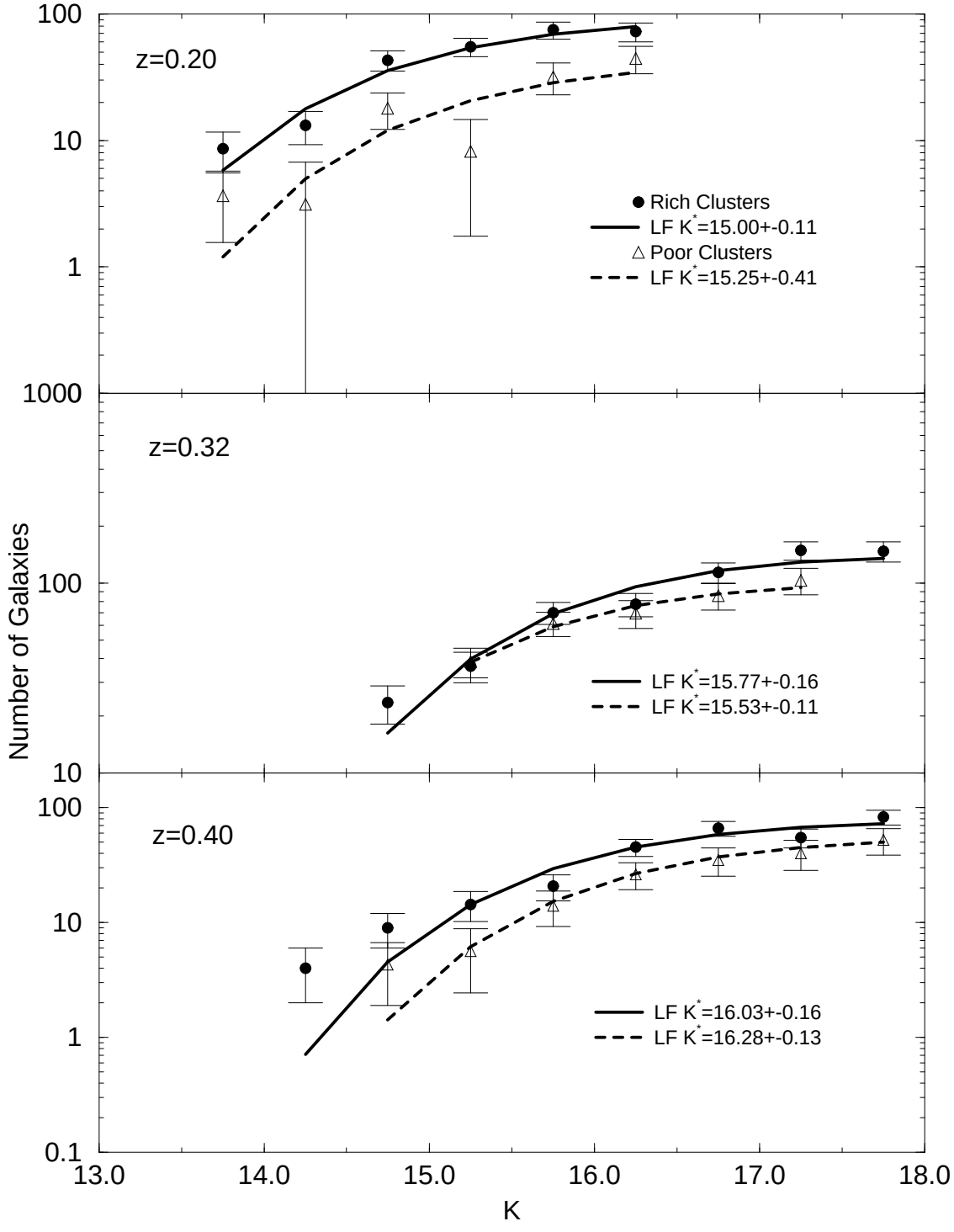

Fig. 7.— (continued)

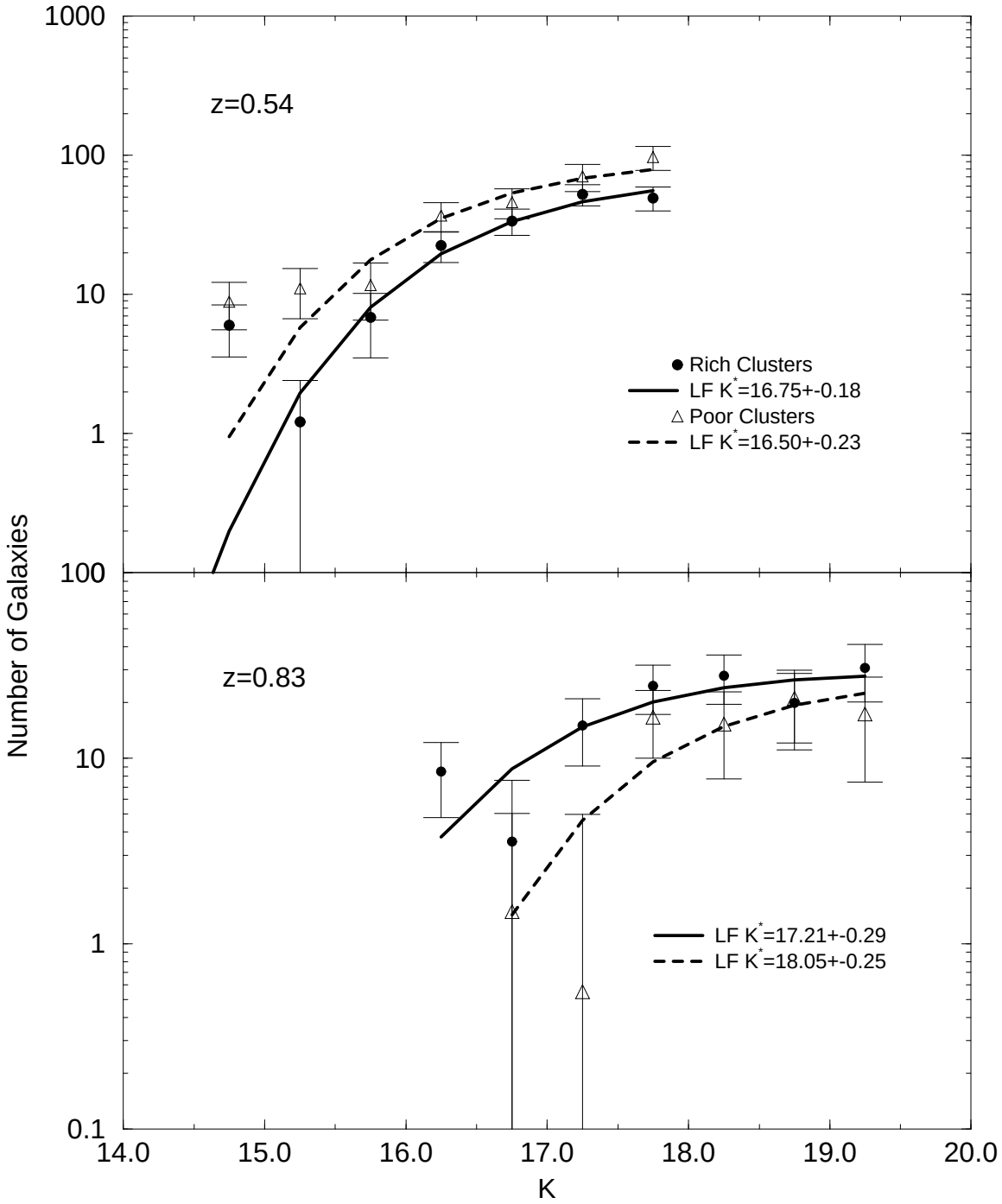

Fig. 8.— K^* vs. z for the cluster sample binned by redshift. Lines represent galaxy models determined from the Bruzual & Charlot GISSEL, normalized to the Coma cluster which has $K^* = 10.9$ (De Propris et al. 1998). These models represent 0.1 Gyr starbursts with a Salpeter IMF and $Z_\odot$, with $H_0 = 65$ km s^{-1} Mpc^{-1}. For the no-evolution cases, the thick solid line is for $\Omega_M = 1$ and $\Lambda = 0$, the thick dotted line is for $\Omega_M = 0.3$ and $\Lambda = 0.7$, and the thick dashed line is for $\Omega_M = 0.3$ and $\Lambda = 0$. For the passive evolution models: the thin solid line represents $z_f = 3.0, \Omega_M = 0.3, \Lambda = 0.7$; the thin dotted line $z_f = 2.0$, $\Omega_M = 0.3, \Lambda = 0.7$; the thin dashed line represents $z_f = 3.0, \Omega_M = 0.3, \Lambda = 0$; and the thin dot-dash line $z_f = 2.0$, $\Omega_M = 0.3, \Lambda = 0$.

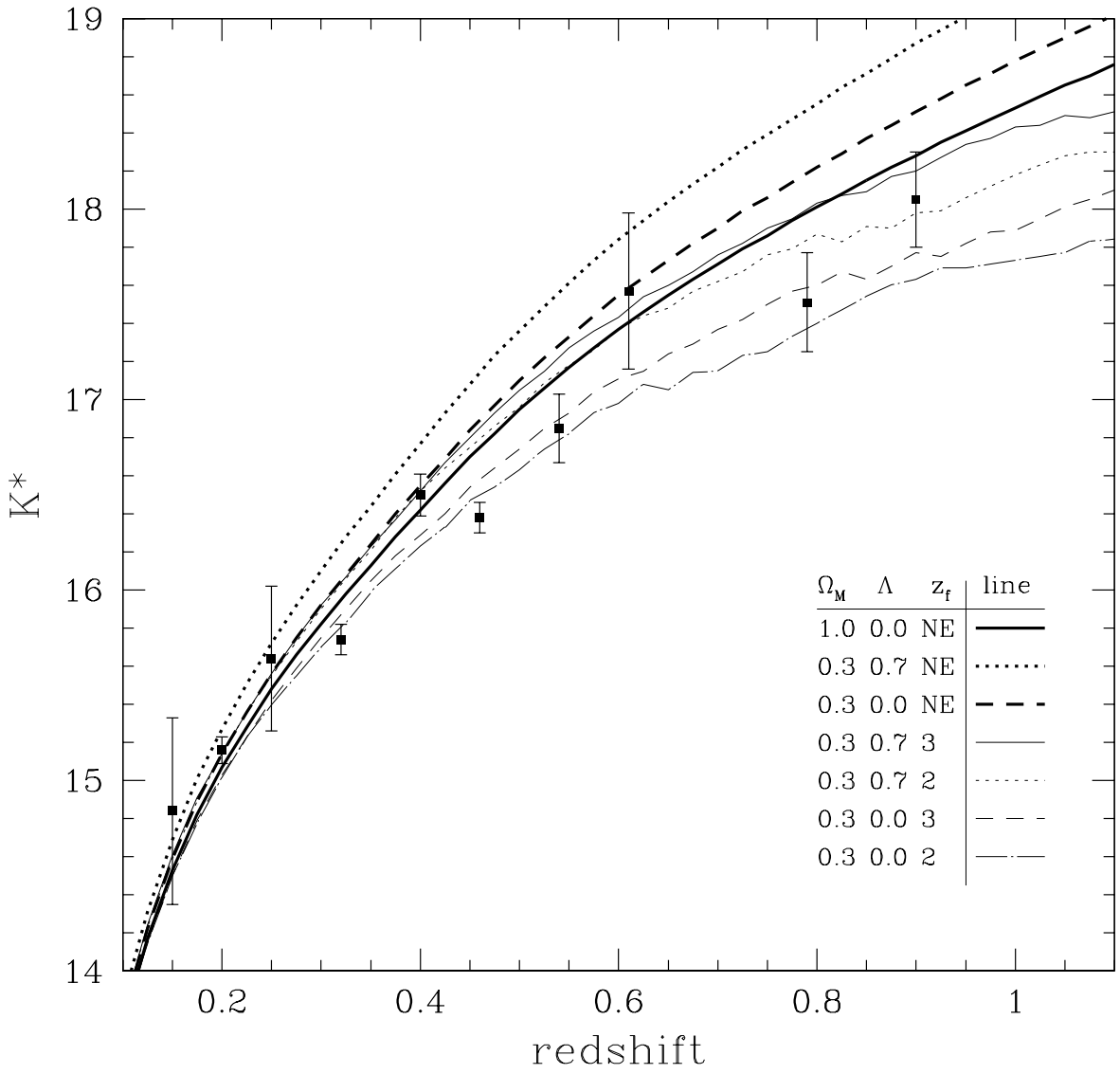

Fig. 9.— K^* vs. z for clusters with high–L_X (solid squares) and low–L_X (open triangles) compared with models for galaxy evolution. The models are the same as those as in Figure 8.

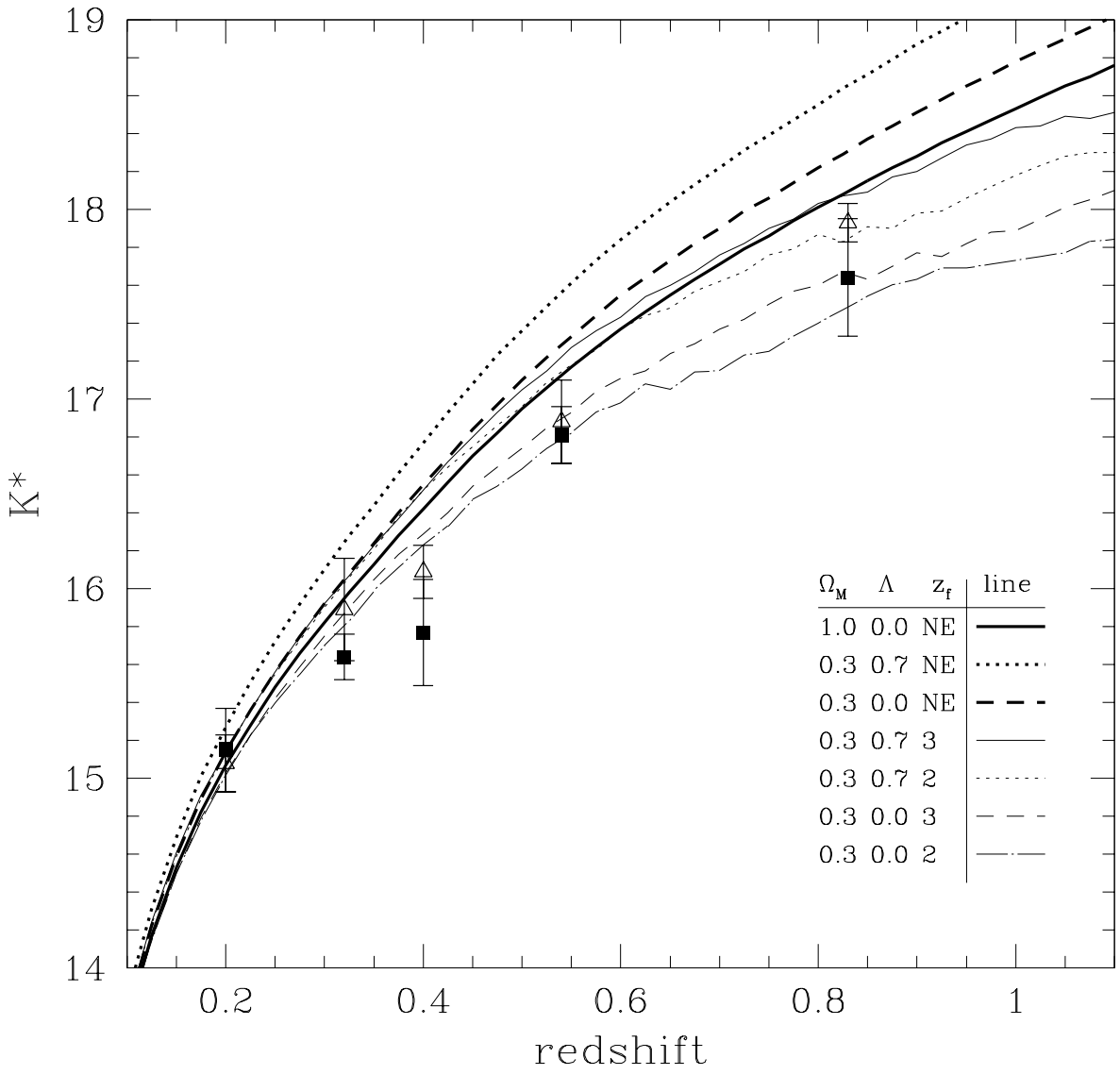

Fig. 10.— K^* vs. z for clusters in the rich (solid squares) and poor (open triangles) subsamples compared with models for galaxy evolution. The models are the same as those as in Figure 8.